HiSST: 3rd International Conference on
High-Speed Vehicle Science Technology
14 -19 April 2024, Busan, Korea

Hypersonic Crossflow-induced Breakdown and Transition Correlation Based on Secondary instability Modes on a Swept Flat Plate

Gen Li[1], Caihong Su[1]

Abstract

Hypersonic crossflow transition was investigated for a Mach 6 flow over a swept plate with a swept angle of 45deg by solving the compressible three-dimensional Navier-Stokes equations. In order to obtain the transition process, the nonlinear evolution of a stationary crossflow vortex was first simulated. After it saturated, broad-spectrum wall perturbations were imposed through a slot to trigger transition. The results showed that both the Type-I and -III secondary modes are excited during the transition, which grow exponentially and independently due to secondary instability. Overall, the Type-I mode achieves the largest amplitude and dominates the transition. Furthermore, the amplitude of the most amplified secondary instability mode based on bi-global analysis is used to correlate the transition locations for DNS cases with four different wall perturbation amplitudes, spanning across four orders of magnitude. It was demonstrated that the amplitude criterion based on secondary instability well correlates the transition locations for the DNS cases, which validates the amplitude criterion based on secondary instability for crossflow transition prediction.

Keywords: Hypersonic, crossflow, boundary layer, transition.

Nomenclature (Tahoma 11 pt, bold)

M – Mach number
ω – Circular frequency
α – Chordwise wavenumber
β – Spanwise wavenumber

Superscripts
∞ – Freestream quantities
Subscripts
r,i – Real and imaginary parts of a complex

1. Introduction

Boundary-layer transition is of high practical relevance in the design of hypersonically flying vehicles. For three-dimensional boundary layers, the crossflow instability arises and may dominate the transition. So far, much of the understanding of the crossflow transition is from low-speed flows. However, the quantitative behavior of the secondary instability was reported to differ markedly between the low-speed and hypersonic flows [1]. In hypersonic flows, the secondary instability is already measurable when the stationary wave saturates and does not grow explosively as in low-speed flows [2]. In the current paper, we are concerned with how the excited secondary instability modes evolve in the transition process, and in particular, we are aimed to verify the transition correlation based on the secondary instability with the different amplitude background disturbances.

2. Model and flow conditions

The boundary layer over a flat plate with a nose radius of 35mm is investigated, as shown in Fig.1. The freestream Mach number is 6 with a sweep angle of 45°. The freestream temperature is 226.5K, and the unit Reynolds number based on freestream variables is 2.26×10^6/m. The nose radius is used as the reference length, and the freestream quantities are used to non-dimensionalize the equations except $\rho_\infty u_\infty^2$ for pressure. The wall is assumed to be no-slip and adiabatic. The base flow and the whole

[1] *Laboratory for High-speed Aerodynamics, Tianjin University, 92 Weijin Rd, Tianjin, China, su_ch@tju.edu.cn*

process of transition was obtained by solving the compressible three-dimensional Navier–Stokes equations with high-order finite difference schemes.

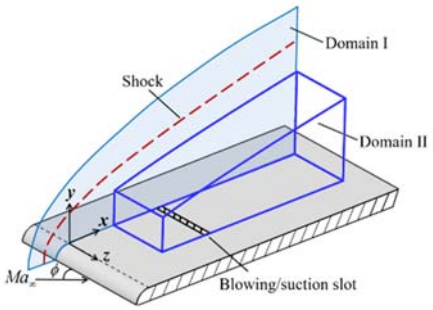

Fig 1. Sketch of the computational setup.

3. Transition induced by stationary crossflow vortices

To obtain the transition, the base flow is first computed in a two-dimensional domain (Domain I in Fig. 1) including the leading edge and the shock. Then, the stationary vortex with β=3 was superimposed on the base flow at x=6 and DNS was performed in Domain II as shown in Fig.1. Its spanwise domain contains one wavelength of the stationary vortex. After the stationary vortex saturates, the wall blowing/suction disturbances with broadband spanwise wavenumbers and frequencies ranging from 1 to 8 (including all the relevant types of secondary instabilities) are imposed at x=36 to trigger transition.

Fig. 2 shows a crosscut of instantaneous temperature contours. As can be seen, initially the stationary crossflow vortices grow and exhibit a typical roll-up structure. Downstream at approximately x=53, small secondary vortices appear, and they grow downstream, eventually leading to transition to turbulence.

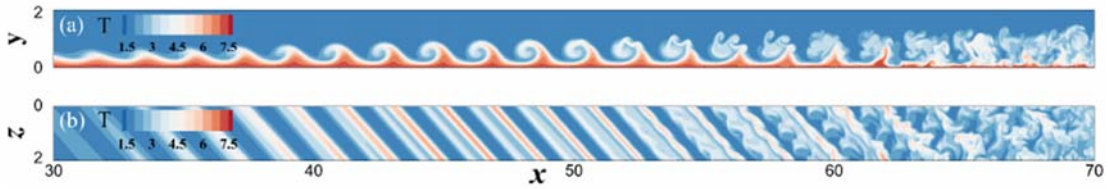

Fig 2. Instantaneous temperature contours (a) in the (x,y) plane at z=0 and (b) in the (x,z) plane at y=0.5.

To shed light on the generated secondary modes, the Fourier analysis was performed on the disturbance time series to obtain the shape functions at each frequency. Meanwhile, taking the flow with the stationary wave as the new mean flow, a local bi-global analysis was performed to obtain the Type-I, -II, and -III secondary instability modes (see Fig.3).

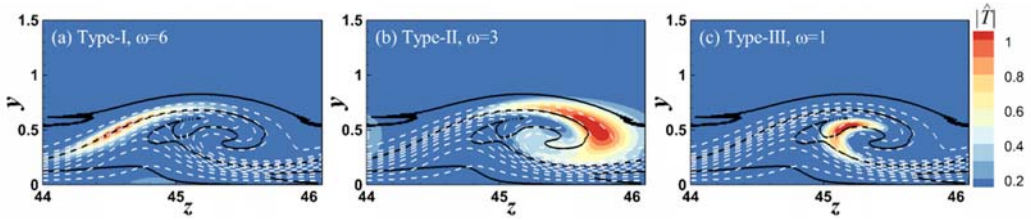

Fig 3. Temperature shape functions of secondary modes at x=40. The white dashed and black solid lines denote the temperature isolines and the generalized inflection points, respectively.

Fig.4 compares the temperature shape functions obtained via Fourier analysis and those from the secondary stability analysis at x=40 and x=45 for the selected frequencies of ω=1,3,6, corresponding to the most unstable secondary Type-III, -II, and -I modes, respectively. As can be seen, at x=40 and for $\omega = 1$, the shape functions of the Type-I (black lines) and Type-III (blue lines) modes agree well with those from DNS, indicating that both modes are excited. In addition, the Type-III mode exhibits larger fluctuations than the Type-I mode, implying its predominance at this frequency. At a higher

frequency of $\omega = 3$, the Type-II mode is expected to occur, but only the Type-I and Type-III modes are identified; the Type-II mode is not observed in the current case despite its amplification predicted by secondary stability analysis. At an even higher frequency of $\omega = 6$, the Type-I mode is seen to be predominant. Similarly downstream at x=45, both the Type-I and Type-III modes coexist at low frequencies. However, as the frequency increases, the Type-I mode becomes increasingly dominant. From the evolution of disturbance amplitudes with different frequencies, as shown in Fig.5, significant growth of secondary instabilities can be seen. Furthermore, two additional DNS cases are performed to obtain the evolutions of the Type-I (ω = 6) and -III mode starting with a small initial amplitude, and the comparison with the DNS results indicates that the excited secondary modes grow exponentially and independently.

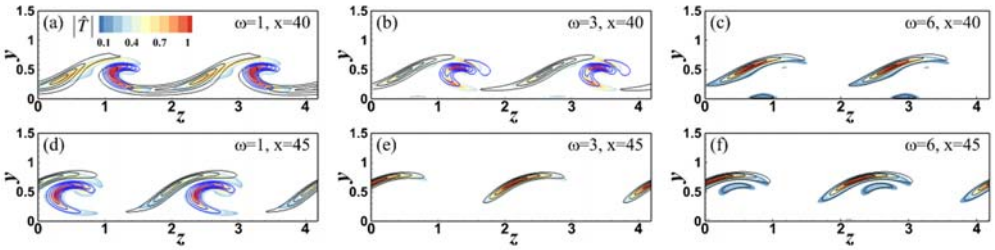

Fig 4. Fourier-transformed temperature shape functions, with black and blue lines denoting the eigenfunctions of the Type-I and -III modes from bi-global stability analysis, respectively.

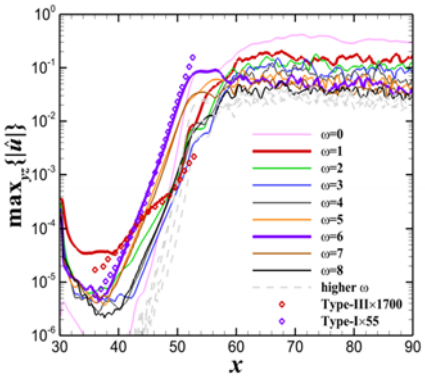

Fig 5. Fourier-transformed amplitude evolution of the chordwise velocity disturbances.

4. Transition correlation based on secondary instability

Since the final breakdown to turbulence is caused by the development of the secondary instabilities of the deformed mean flow, it is natural to link the transition location to secondary instability. The amplitude of a secondary instability mode can be written as

$$A = A_0 e^N = C A_\infty e^N \tag{1}$$

where A_0 denotes the initial amplitude of the excited secondary mode, A_∞ is the amplitude of the wall blowing/suction disturbances and C is the receptivity coefficient. Here, N represents the amplification ratio of the most amplified secondary mode, which is computed by accumulating the growth rate obtained from the bi-global analysis.

For the same type of external forcings, the receptivity coefficient should be the same. Thus, it can be moved to the left hand of Eq. (1) and considered with the amplitude A together:

$$A' = A/C = A_\infty e^N \tag{2}$$

Similar to Mack's amplitude method, we use $A' = A_{tr}$ to correlate the transition location. Note that A' is a parameter, which no longer represents the disturbance amplitude. We now consider four DNS cases with different A_∞, ranging from 4×10^{-5} to 4×10^{-2}. The friction coefficient for the four cases is shown in Fig. 6, also included is a rectangle whose left and rights side mark the predicted transition locations by $A' = 4, 5$, respectively. As can be seen, this amplitude criterion well correlates the transition locations for the DNS cases. In addition, referring back to Fig. 5, C can be determined as 0.015, and

corresponding to A'=4 and 5, A in Eq. (2) is 0.06 and 0.075, respectively, which are reasonable values for a disturbance amplitude.

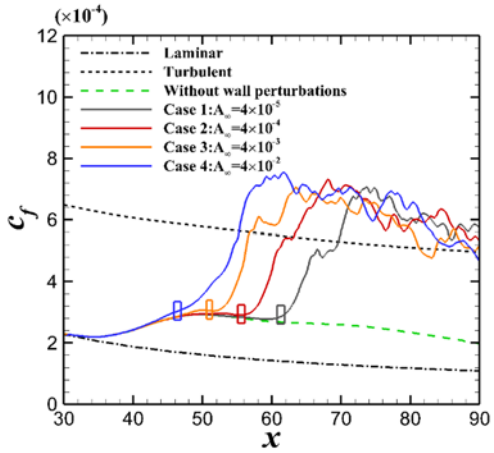

Evolution of averaged skin friction coefficient and the left and right sides of the small rectangles mark the predicted transition positions based on A'=4 and 5, respectively.

5. Conclusion

In this paper, the boundary layer transition induced by a stationary vortex is investigated using direct numerical simulations for a Mach 6 flow over a swept plate with a swept angle of 45deg. To obtain the transition process, the nonlinear evolution of a stationary crossflow vortex is first simulated, and then broad-spectrum wall perturbations are imposed through a slot to trigger transition. We found that during the transition process, both the Type-I and -III secondary modes are excited. In contrast, the Type-II mode is not detected despite its amplification predicted by global analysis. Before the transition onset, and the excited secondary modes grow exponentially and independently. Overall, the Type-I mode achieves the largest amplitude and dominates the transition. In addition, the transition process is obtained simulated with four different initial amplitudes of wall blowing/suction disturbances, spanning across four orders of magnitude. It was shown that the amplitude of the secondary instability mode based on bi-global analysis is able to well correlate the transition locations. This work promotes the understanding of crossflow transition and validates the transition criterion based on secondary instability in hypersonic boundary layers.

References

1. Saric, W. S., Reed, H. L., White, E. B.: Stability and transition of three-dimensional boundary layers. Annual Review of Fluid Mechanics, 35(1): 413-440 (2003)
2. Kocian, T. S., Moyes, A. J., Reed H. L., et al.: Hypersonic Crossflow Instability, Journal of Spacecraft and Rocket. 56(2): 432-446 (2019).